Nanoscale

Microenvironment Control of Porphyrin Binding, Organization, and Function in Peptide Nanofiber Assemblies

Journal:	*Nanoscale*
Manuscript ID	NR-ART-11-2018-009556.R1
Article Type:	Paper
Date Submitted by the Author:	29-Jan-2019
Complete List of Authors:	Solomon, Lee; Argonne National Laboratory Wood, Anna; Emory University - Briarcliffe Campus Sykes, Matthew; Argonne National Laboratory Diroll, Benjamin; Argonne National Laboratory, Center for Nanoscale Materials Wiederrecht, Gary P.; Argonne National Laboratory Schaller, Richard; Argonne National Laboratory, Center for Nanoscale Materials Fry, Harry; Argonne National Laboratory, Center for Nanoscale Materials

Microenvironment Control of Porphyrin Binding, Organization, and Function in Peptide Nanofiber Assemblies

Lee A. Solomon[1], Anna R. Wood[1], Matthew E. Sykes[1], Benjamin T. Diroll[1], Gary P. Wiederrecht[1], Richard D. Schaller[1,2], and H. Christopher Fry[1]*.

[1]Center for Nanoscale Materials, Argonne National Laboratory, Lemont, IL 60439 United States

[2]Department of Chemistry, Northwestern University, Evanston, IL 60208, United States

ABSTRACT: To take peptide materials from predominantly structural to functional assemblies, variations in cofactor binding sites must be engineered and controlled. Here, we have employed the peptide sequence c16-AH$\mathbf{X_3}$K$_3$-CO$_2$H where $\mathbf{X_3}$ represents the aliphatic structural component of the peptide design that dictates β-sheet formation and upon self-assembly yields a change in the overall microenvironment surrounding the Zn protoporphyrin IX ((PPIX)Zn) binding site. All peptides studied yield β-sheet rich nanofibers highlighting the materials' resiliency to amino acid substitution. We highlight that the (PPIX)Zn binding constants correlate strongly with amino acid side chain volume, where X = L or I yields the lowest dissociation constant values (K_D). The resulting microenvironment highlights the materials' ability to control interchromophore electronic interactions such that slip-stacked cofacial arrangements are observed via exciton splitting in UV/visible and circular dichroism spectroscopy. Steady state and time-resolved photoluminescence suggests that greater interchromophore packing yields larger excimer populations and corresponding longer excimer association lifetimes (τ_A) which directly translates to shorter exciton diffusion lengths. In comparison to synthetic porphyrin molecular assemblies, this work demonstrates the ability to employ the peptide assembly to modulate the degree of cofactor arrangement, extent of excimer formation, and the exciton hopping rates all while in a platform amenable for producing polymer-like materials.

Introduction

Biomaterials for light harvesting applications are sought after in the photosynthetic and photovoltaic communities owing to their ability to harvest economical and environmentally sustainable solar energy.[1] Proteinaceous systems have a tunability and repair potential that far outcompetes their synthetic counterparts. Nature performs light capture via careful and precise arrangement of multiple chromophores (e.g. chlorophyll) in an organized protein array.[2-5] Some groups employ these light activated proteins in various nanotechnology assemblies and devices.[6, 7] However, tailoring these proteins for optimal device performance can be problematic due to the complexity of the protein structure.

Many efforts have been made toward emulating light harvesting proteins while avoiding the complications of natural proteins. Supramolecular arrangements of chromophore systems, like porphyrins and donor-acceptor molecules have produced some excellent examples of artificial light harvesting and photocatalytic systems.[8-10] While this approach has produced an abundance of excellent materials and greatly opened the field of light harvesting supramolecular arrays, the assemblies often lose the precision and architecture of the protein and its ability to precisely orient the molecules as well as provide a unique microenvironment that modulates the properties of the light harvesting function. Ignoring these effects limits their functional potential, removing the ability to tune the properties. Another approach that addresses chromophore placement precision and microenvironment involves the modification of existing proteins creating supramolecular protein assemblies.[11] The examples of supramolecular heme proteins reviewed by Oohora et al., could be applied to artificial light harvesting proteins via heme substitution with zinc protoporphyrin IX. In fact, nature employs supramolecular assemblies for light harvesting as evidenced by the high resolution structures of photosystem II and light harvesting complex II, highlighting a crystalline array of the proteins embedded in a lipid bilayer

with highly ordered cofactors.[4, 5] Peptide self-assembly offers a medium between protein assemblies and chromophore assemblies.[12]

Our group has developed artificial multi-chromophore peptide-amphiphile arrays. The material is self-assembling and capable of not only axially coordinating metalloporphyrins but also orienting the molecules with respect to the axis of the resulting nanofiber.[13, 14] As a result, the small peptide presents a platform in which the photophysical properties of the resulting assembly can be modified either through a change in cofactor or, as we explore here, a change in environment by varying the peptide sequence. Variations in the sequence can lead to both gross morphological changes as well as a change in the microenvironment surrounding the chromophores. Thus, our work avoids the pitfalls of natural proteins and synthetic multi-chromophore systems as materials.

The peptide, c16-AHL_3K_3-CO_2H, was previously designed[13] with a few basic criteria: (1) a histidine placed close to the hydrophobic interior of the assembly for axial transition metal coordination, (2) a positively charged head group to yield a high pH trigger for assembly, and (3) a moderate propensity β-sheet conformer, like leucine, to prevent the molecule from spontaneously self-assembling into β-sheet rich nanofibers. The peptide assembles into β-sheet rich nanofibers upon increasing the pH above the pK_a of the lysine residues. Here, we explore the variation of the "β-sheet region" of the peptide sequence where we change the L_3 segment to a series of peptides containing the general sequence, c16-AH$\mathbf{X_3}K_3$-CO_2H, where X denotes any of the six hydrophobic amino acids. This systematic variation allows us to probe the effects of amino acid side chain volume, and binding site environment on: (1) the resulting assembly morphology, (2) the ability to axially coordinate the photoactive metalloporphyrin, zinc protoporphyrin IX (PZn), (3) the interchromophore interactions, and (4) the photophysical properties of the chromophore assembly. With respect to the photophysical properties, we recently reported on the exciton diffusion length (L_d) and how it was limited by the formation of

excimer complexes.[14] We report here that instead of changing the chromophore to achieve desired photophysical properties like longer exciton diffusion lengths, we can simply modify the peptide sequence changing the microenvironment surrounding the chromophore array. This imparts a change in the photophysical behavior, e.g. rate of formation of the excimer complex. Overall we highlight that our system merges the scalability and simplified structure of synthetic porphyrin assemblies with the tunability of natural proteins.

Results and Discussion

Design and Visualization In an effort to probe the role of the microenvironment on the binding and photophysical properties of (PPIX)Zn to a series of self-assembling peptide amphiphiles, we employed the sequence from our earlier work, c16-AH**X_3**K_3-CO_2H, where c16 is a palmitoyl chain. The histidine is utilized in axial coordination of the metalloporphyrin unit. Lysine was chosen as a pH trigger for self-assembly where upon increasing the pH of the solution, electrostatic repulsion is reduced allowing neighboring molecules to readily interact. The overall supramolecular assembly yields a nanofiber with a diameter of ~7 – 9 nm where the (PPIX)Zn molecules are aligned along the length of the peptide fiber, Figure S1. Here, we have varied the hydrophobic, β-sheet segment **X_3** in an effort to probe the effects of amino acid side chain volume on assembly, binding affinity and photophysical properties. Figure 1 highlights the order of increasing amino acid side chain volume from Ala<Val<Leu,Ile<Phe<Trp.[15] Throughout this report, we refer to the peptides strictly by the β-sheet segment, e.g. c16-AHV_3K_3-CO_2H = V_3.

Energy minimization studies of small segments of the assemblies using CHARMM force fields were employed to visualize the effect that increasing the amino acid side chain volume would have on (PPIX)Zn coordination, Figure 1. Amino acid side chain volume can not only affect the chromophore packing environment, but it could also influence the number of accessible histidine rotamers ultimately impacting the chromophore binding affinity, Figure S2.[16, 17] We aligned seven peptides in a parallel β-sheet assembly arrangement and coordinated the Zn metal center of one (PPIX)Zn molecule to the δ-nitrogen of a histidine. While all peptides maintained a β-sheet arrangement, it was evident that the impact of the volume of the side chain residues was significant. The A_3 assembly yields an underpacked binding site as indicated by the void between the methyl side chain and the porphyrin plane which allows the (PPIX)Zn to tilt freely. This is in contrast to W_3 in which steric repulsion was observed between the indole side chain and the chromophore effectively pushing (PPIX)Zn away from the coordination site. L_3 and I_3, on

the other hand, indicate packing interactions between the chromophore and the peptide where the side chains are neither sterically repelling nor underpacking the binding site.

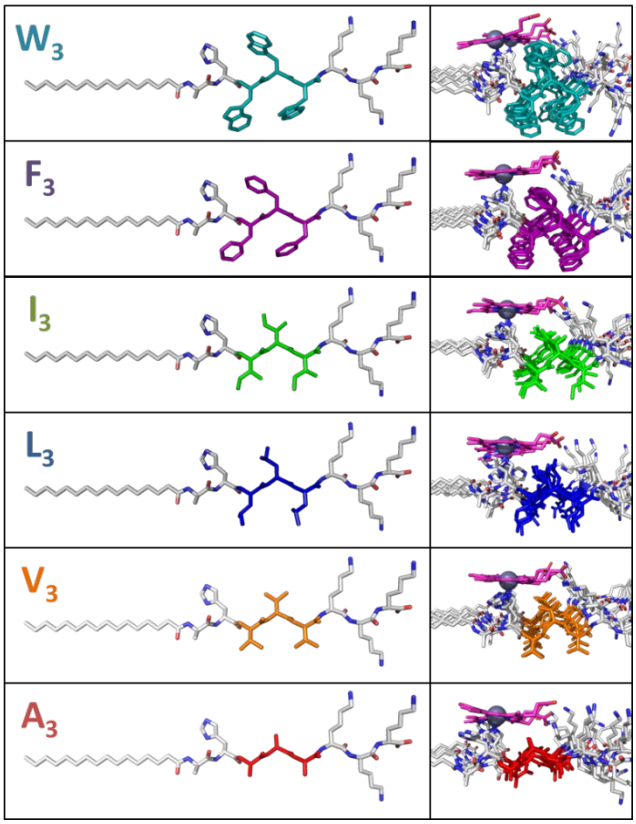

Figure 1. Peptide designs following the sequence c16-AHX_3K_3-CO_2H where X = A (red), V (orange), L (blue), I (green), F (purple), W (cyan). The panel on the right highlights heptameric parallel β-sheet assemblies with a histidine coordinated (PPIX)Zn molecule in magenta (Hyperchem 8.0: energy minimized structures, *in vacuo*, CHARMM27; Pymol: visualization and color coding).

Material Assembly and Characterization Prior to porphyrin binding, we examined the self-assembly properties of the peptides alone. To trigger self-assembly, we prepared a 500 μM solution of peptide and increased the pH to ~11 by adding ammonium hydroxide (30 mM). We then dilute this solution into water tenfold and analyzed the secondary structure with both circular dichroism spectroscopy and infrared spectroscopy, Figure S3. At this pH, all peptides

were observed to form β-sheets regardless of propensity. β-sheets are typically characterized by signature amide I vibrations determined by infrared spectroscopy,[18] ν = 1627 and 1681 cm^{-1} and a signature electronic transition at 218 nm in circular dichroism spectroscopy. The CD spectra of the peptide assemblies indicate that the MRE at 218 nm varies between 11,000 and 19,000 deg cm^2 $dmol^{-1}$ res^{-1}. In addition, there are slight variations in the 218 nm transition that are sometimes attributed to gross supramolecular ordering, e.g. superhelical twist yields a red-shift.[19] W_3 appears unique at first glance, but the tryptophan molecule contribute significantly to the absorption in this region yielding a positive Cotton effect at λ = 228 nm and negative Cotton effect at λ = 210 nm. However, the FTIR data suggests the formation of *β*-sheets although the relative intensities of the 1627 and 1681 cm^{-1} frequencies are modulated in comparison to the other peptide assemblies.

Although not mutually exclusive, β-sheet formation can be an indication of fiber formation. We utilize transmission electron microscopy to evaluate the morphology of the resulting self-assembled material, Figure 2. In all cases, fibers are formed. In fact, for A_3, V_3, L_3, and I_3 the morphologies are nearly identical in that individual fibers tend to bundle together. However, F_3 and W_3 seem to form more aggregated structures of fibers as opposed to aligned bundles. This is potentially due to the aromatic nature of the phenylalanine and tryptophan that provide another route of aggregation via π–π interactions that does not exist for the other peptides studied here. Furthermore, W_3 is more aggregated than F_3 which makes additional characterization difficult as sample scattering can interfere with data interpretation. It should be noted that addition of (PPIX)Zn does not influence secondary structure or morphology.

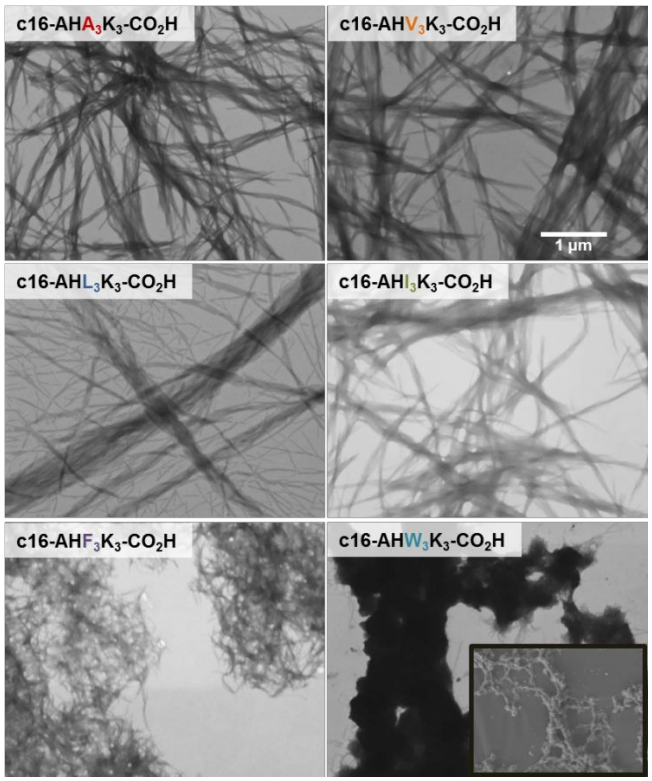

Figure 2. Transmission electron micrographs of c16-AHX_3K_3-CO_2H (scale bar = 1 μm). The inset for c16-AHW_3K_3-CO_2H is a scanning electron micrograph highlighting the aggregated fibers.

The ability for all peptide assemblies to yield a one dimensional, β-sheet rich, nanofiber assembly demonstrates a structural resiliency upon variation of the X_3 block. Upon addition of binding (PPIX)Zn to the various peptide assemblies, we employ a variety of spectroscopies to investigate the binding affinity, inter-chromophore interactions, and photophysical properties. First, we utilize UV/visible spectroscopy to observe the binding of (PPIX)Zn to the different peptide assemblies, Figure 3. Titration experiments are performed where we begin with a 5 μM (PPIX)Zn solution in 30 mM ammonium hydroxide (3 mL) in a 1 cm quartz cuvette and add 5 μM aliquots of peptide fibers. We collected UV/vis spectra while increasing the ratio from 1:1 to 20:1

peptide:(PPIX)Zn. The increasing absorption value for the Soret peak (λ_{max} = 425 – 431 nm) is analyzed using eq. S1 (Supporting Information) in which the dissociation constant (K_D) and stoichiometric ratio (n = peptide:(PPIX)Zn or how many peptides it takes to bind one (PPIX)Zn molecule) are determined. In each analysis where K_D < 2 μM (i.e. V_3, L_3, I_3, F_3), the ratio was noted to be ~6(±0.5):1. In order to compare the series of peptides, the reported K_D values represent the results where we fixed the ratio to 6:1. In all cases, (PPIX)Zn was able to bind to the peptide assembly with affinities varying over nearly two orders of magnitude (0.2 to 16 μM).

In an effort to determine why there was a variation in binding constant, the resulting K_D values were plotted against amino acid side chain volumes, Figure 3.[15] L_3 (K_D = 0.23 μM) and I_3 (K_D = 0.31 μM) were found to provide the best packing environment (amino acid side chain volumes ~170 Å^3) for the porphyrin molecules. Consistent with our molecular models, A_3 (K_D = 16 μM) does not provide a well packed binding site for (PPIX)Zn coordination whereas W_3 (K_D = 14 μM) produces an overpacked binding that yield high dissociation constants/low binding affinity. Our supposition that amino acid volume as a parameter for dictating binding affinity is further supported by the fact that V_3 (K_D = 0.78 μM) which is slightly underpacked and F_3 (K_D = 1.09 μM) which is slightly overpacked yield intermediate binding constants.

With these gradual changes in amino acid substitution, we find a direct influence on the (PPIX)Zn binding constant that is directly related to amino acid side chain volume. Therefore, we suggest that our current design strategy for developing self-assembling peptide materials that are functionalized with the photoactive chromophore (PPIX)Zn demonstrates some resiliency to sequence variations with a demonstrably tunable binding site affinity.

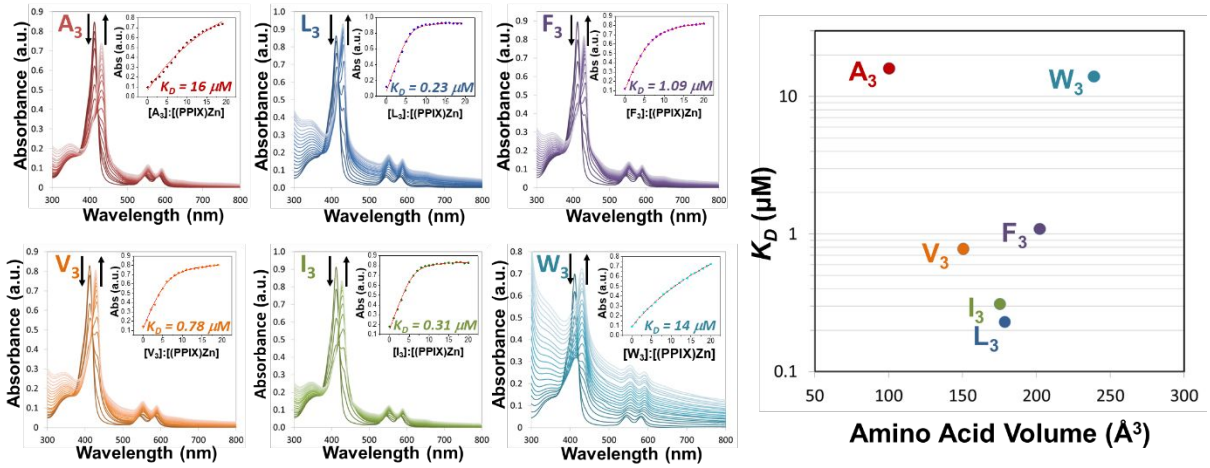

Figure 3. UV/visible spectroscopic titration experiments in which 5 μM aliquots of peptide were added to a 5 μM solution of (PPIX)Zn in 30 mM NH_4OH. The insets represent binding analysis (K_D) at λ_{max} of (PPIX)Zn bound to peptide where the peptide:(PPIX)Zn was varied from 1:1 to 20:1. c16-AHX_3K$_3$-CO_2H:(PPIX)Zn binding constant plotted against amino acid volume. A_3 (red), V_3 (orange), L_3 (blue), I_3 (green), F_3 (purple), W_3 (cyan).

Designing peptides for metalloporphyrin coordination/incorporation[12, 20] is a well-studied field and continues to grow with recent highlights incorporating larger, abiotic porphyrin based donor-acceptor and push-pull molecules.[21-23] All of these examples, however, are helical bundles. Despite the differences between secondary structure of our presented β-sheet rich peptide assemblies and the helical bundles, the local environment surrounding the metalloporphyrin is quite similar. For example, the planar nature of the metalloporphyrin renders it hydrophobic and therefore requires a hydrophobic binding site. However, as demonstrated here, amino acid side chain volume is a critical parameter such that random selection of an aliphatic amino acid is inadequate. Consistent with the helical designs, leucine and isoleucine represent the commonly occurring amino acids that lay adjacent to the axially coordinating histidine and offer the best molecular packing between the peptide side chains and the metalloporphyrin macrocycle,

Figure S4 and Table S1.[21-30] Distal sites of PZn binding peptide assemblies also typically employ isoleucine or leucine. Therefore, by placing these two amino acids proximally to the binding site of PZn, we achieve the highest binding affinity consistent with results from empirical and first principles derived helical peptide designs.

In nature, the ubiquity of chromophores like chlorophyll and heme in energetic processes is critical for cellular function.[31, 32] Engineering materials that utilize not only the energetic capabilities of the chromophores but also the necessary environment of the protein for proper function is a major challenge. In an effort to generate novel materials, many take the opportunity to immobilize existing proteins (natural or *de novo* designed) on substrates using well-established bioconjugation methods, e.g. self-assembled monolayers.[33, 34] The supramolecular scaffold of a peptide amphiphile, most typically used in drug delivery and regenerative medicine, has been demonstrated to behave like a polymer.[35] The resulting material, therefore, has advantages towards being employed and processed like many of the peptide amphiphiles previously reported. To afford efficient and stable assemblies useful in energy related research, we utilize cofactors as the primary functional unit such that demonstrating the ability to tune the chromophore affinity and function through peptide sequence variation is essential in highlighting the role of the nanoscale assembly. The unique influence of the nanoscale assembly becomes apparent when investigating the ability to spatially control an array of chromophores in the X_3 peptide series.

Probing Interchromophore Interactions As noted in our previous work, the interchromophore interactions play a critical role in the photophysical properties of the material.[14] Under low peptide:porphyrin ratios (i.e. densely packed porphyrin within a single peptide fiber), a high degree of excimer formation was observed that limited the diffusivity of the delocalized exciton. As the ratio is increased (i.e. fewer porphyrin molecules are loaded in the fibers), the diffusivity increases due to a decrease in excimer formation. The excimer was identified in a detailed time

resolved photoluminescence study and confirmed in the steady-state spectra as well. Here, changes in the structural β-sheet region (i.e. the microenvironment surrounding the chromophore) were found to significantly affect the rate of excimer formation.

UV/visible spectroscopy of the entire series reveals bound chromophores to each peptide assembly, Figure 3. However, the λ_{max} of the Soret band varies from 422 to 431 nm depending on the sequence, Figure 4. For example, L_3:(PPIX)Zn yields a split Soret (422 and 431 nm) that we attribute to a slipped cofacial arrangement of neighboring chromophores.[36] We expected to observe similar results with varying degrees of the split Soret signature, but all other peptides yield Soret bands centered on a single wavelength. The two peaks are not due to a mixture of uncoordinated and coordinated (PPIX)Zn as the uncoordinated molecule yields λ_{max} = 412nm. When histidine is mixed with (PPIX)Zn it yields λ_{max} = 421 nm. We therefore attribute the red shift in the electronic spectra to the peptide mediating aggregation of (PPIX)Zn.

The circular dichroism spectra of the coordinated (PPIX)Zn comment on how well organized the neighboring chromophores are in the peptide amphiphile nanofibers. For example, if the molecules are in a chiral environment, regularly spaced, with a fixed dihedral angle they will yield a very intense spectrum.[37, 38] These phenomena are reported in the chlorophyll organizing proteins, PS II and LH2.[39, 40] If the molecule is coordinated, but cannot be fixed into a specific arrangement, e.g. the dihedral angle between neighboring chromophores is random, chiroptical activity will not be observed. As a result, it is interesting to note that the peptide, L_3, which yields a split Soret, also yields the most intense CD spectrum indicating that out of all of the peptides investigated here, L_3 demonstrates the greatest ability to organize (PPIX)Zn. All peptide:(PPIX)Zn assemblies, with the exception of W_3, exhibit a CD response, but the signal intensities are more than tenfold less than that of the leucine containing peptide suggesting that while they may be bound in the fibers, they are not as well organized (e.g. yielding a broad range of interchromophore dihedral angles) as L_3.

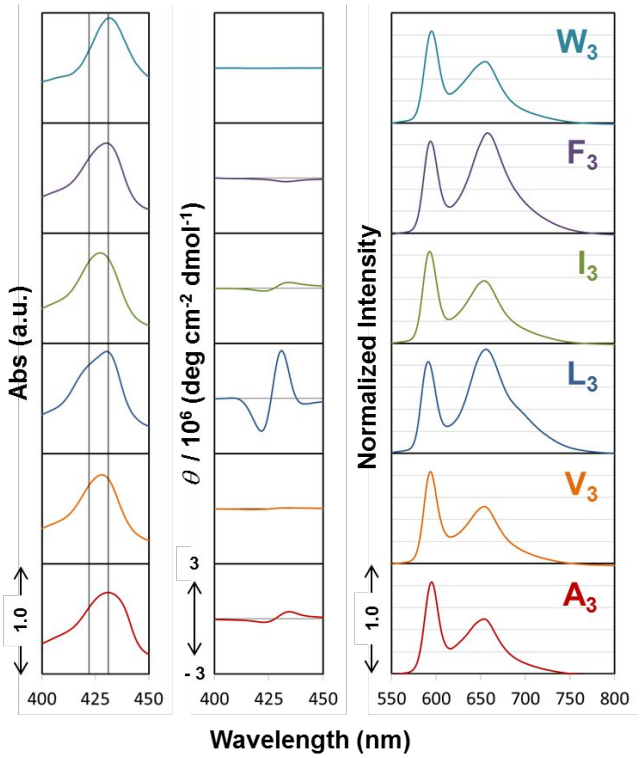

Figure 4. Data representing 10:1 c16-AHX_3K_3-CO_2H:[(PPIX)Zn]. A. UV/visible spectroscopy of the Soret region, B. circular dichroism spectroscopy of the Soret region, and C. steady state emission spectroscopy measurements (λ_{ex} = 425 nm). A_3 (red), V_3 (orange), L_3 (blue), I_3 (green), F_3 (purple), W_3 (cyan).

Fluorescence spectroscopy provides additional evidence towards interchromophore interactions (Figure 4). Steady state fluorescence spectroscopy was monitored in parallel with UV/vis spectroscopy during the titration experiments, Figure S5. In every titration, we observed similar behavior. First, the monomeric (PPIX)Zn molecule in 30 mM NH_4OH without peptide yields a typical singlet spectrum with fluorescence S1→S0 bands at 590 and 650 nm. In this singlet state, the intensity at 590 nm is greater than that of 650 nm. Upon addition of peptide, the

fluorescence dramatically decreases. The observed quenching “bottoms out” at the ideal concentration of peptide:porphyrin, 6:1, Figure S4. This suggests that at the greatest loading capacity of porphyrin in the peptide assembly, the interchromophore interactions are at their greatest. Next, upon additional increase of peptide concentration, the porphyrins begin to become spatially separated which results in an increase of the fluorescence signal of coordinated (PPIX)Zn as the interaction between neighboring chromophores decreases. Furthermore, we have previously characterized an excimer species in the L_3:(PPIX)Zn complex that is centered at ~680 nm. As a result, the observed steady state spectrum is a mixture of the singlet and the excimer states in the steady state fluorescence spectra such that the 650nm emission appears more intense than the 590 nm emission. The excimer is most easily observed in the steady state spectrum for L_3 and F_3 (Figure 4), but in all other spectra it is greatly reduced as noted by the lower intensity of the spectra at 680 nm.

Photophysical Phenomena Zinc porphyrins have been used in the photoinitiation of electron transfer,[41] dye-sensitized solar cells[42], artificial light harvesting assemblies[9], and in photodynamic therapy.[43] As a result, a fundamental understanding and comparison of the photophysical behavior of PZn molecules in various assemblies is necessary. A zinc porphyrin molecule, upon visible light excitation, immediately forms a singlet excited state that undergoes intersystem crossing to form a triplet state which decays back to the ground state. This simple model is disrupted when the chromophore is placed in a protein environment. For example, when (PPIX)Zn is coordinated to the hemin binding site of myoglobin (Mb), the photodynamics in the singlet manifold are altered.[44] Through multiexponential analysis, (PPIX)Zn:Mb yields three decay components: (1) τ_1 ~ 700 fs a hot S1 state that transfer energy to Mb through the dative bond between (PPIX)Zn and histidine, (2) τ_2~30 ps reflects the transfer of vibrational energy from (PPIX)Zn to water in the Mb binding pocket, and (3) the long and dominant τ_3 ~2

ns component reflects intersystem crossing to form the triplet (S1→T1). The ability to undergo intersystem crossing is reliant on the protein binding (PPIX)Zn in a discrete pocket.

In light harvesting systems, the protein structure organizes multiple chlorophyll molecules with great spatial precision. As a result, significant efforts have been made to control the aggregation and self-assembly of PZn molecules through carefully designed and synthesized molecules.[45] Synthetic PZn aggregates rely on π-stacking or covalently attached coordination ligands to control molecular organization. Exciton interactions between neighboring molecules in "slip-stacked" cofacial arrangements lead to the formation of excimers and exciplexes that exhibit a broad range of picosecond lifetimes that are highly dependent on relative porphyrin orientation (i.e. coplanar vs. orthogonal orientation). The lifetimes are often attributed to exciton hopping.

Our series of peptides offers a unique "in-between" state for these given examples of (PPIX)Zn:Mb and PZn aggregates. That is, the peptide assembly yields a network of (PPIX)Zn molecules like the PZn assemblies but in a protein like environment where secondary interactions with the side chains of the amino acids can influence the spatial orientation of neighboring molecules. As such, the X_3 peptide series facilitates the ability to probe whether the degree of ordering or the local microenvironment yields a greater impact on various photophysical phenomena like exciton diffusion and excimer formation. Time resolved photoluminescence spectroscopy of the X_3 series (Figure 5) confirms the formation of an excimer complex on the picosecond timescale in all peptides. Upon excitation (λ_{ex} = 425 nm), we observe a typical emission spectrum of the singlet excited state of PZn at the earliest delay times (<100 fs). After the formation of the singlet state a competitive pathway occurs. The singlet either decays monoexponentially to the ground state ($\tau_{Singlet}$), or it associates with a ground state (PPIX)Zn (τ_a) forming the excimer complex, as indicated by the biexponential decay at 590 nm. The excimer complex forms (τ_a) and then decays ($\tau_{Excimer}$) back to the ground

state, as indicated by the biexponential rise and decay at 680 nm. It should be noted that the formation of the excimer prevents intersystem crossing as evidenced by supporting transient absorption data showing significantly diminished triplet formation, Figure S6.

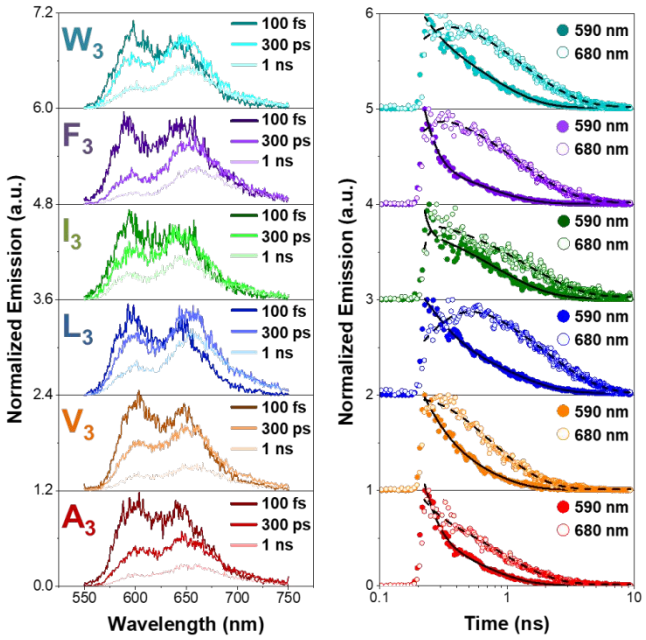

Figure 5. Time resolved photoluminescence spectroscopy of c16-AHX_3K_3-CO_2H:(PPIX)Zn (10:1). A. Emission spectra at time delays < 100 fs (earliest times, dark colored lines), 300 ps (colored lines), and 1 ns (light colored lines) highlighting the shift from singlet to excimer emissive states. B. Pico- to nanosecond resolved kinetics monitored at wavelengths 590 nm (circles) and 680 nm (open circles). Biexponential kinetic fits of 590 nm (solid line) and 680 nm (dashed line) highlighting the wavelength dependent kinetics. Lifetime values (τ_a, $\tau_{Singlet}$, and $\tau_{Excimer}$)_reported in Table 1. A_3 (red), V_3 (orange), L_3 (blue), I_3 (green), F_3 (purple), W_3 (cyan).

Peptide	τ_a (ps)	$\tau_{Singlet}$ (ns)	$\tau_{Excimer}$ (ns)	L_D (nm)
A_3	65	0.51	0.9	9.9
V_3	104	0.48	0.7	6.5
L_3	145	0.93	2.0	6.5
I_3	20	0.77	1.4	8.8
F_3	57	0.59	1.3	8.5
W_3	90	0.67	1.4	5.4

Table 1. Lifetime data from TRPL biexponential analysis at wavelengths 590 nm and 680 nm. At 590 nm lifetime measurements for τ_a and $\tau_{Singlet}$ are determined and at 680 nm, lifetime measurements for τ_a and $\tau_{Excimer}$ are determined. τ_a was determined from data at both wavelengths 590 and 680 nm. Diffusion lengths (L_D) were determined as described in ref 14.

While the steady state emission spectra (Figure 4) visibly indicate excimer formation in L_3 and F-$_3$, the time resolved data makes it apparent that the (PPIX)Zn excimer species forms in all peptide assemblies at varying rates. Emission spectra at various time delays highlight the preliminary formation of the monomer and competitive conversion to the excimer (when the peak is more intense at 650 – 680 nm than 590nm) (Figure 5). The monomer to excimer transition is most evident in L_3, I_3, F_3, and W_3 due to the resolvable rise times in the kinetics at λ = 680 nm. The measured rate constants (τ_a, $\tau_{Singlet}$, and $\tau_{Excimer}$) vary with respect to the peptide studied and are summarized in table 1.

We previously identified, through a more rigorous global analysis using a 1D exciton diffusion model that the formation of the excimer severely limits the diffusion length (L_D) of the electron/hole pair as the excimer offers a pathway of charge recombination.[14] We determined this by varying the amount of (PPIX)Zn that we added to the assembled fibers of c16-AHL_3K_3-CO_2H. As we decreased the amount of (PPIX)Zn we observed an increase in diffusion length that was inversely proportional to the amount of excimer that was formed. Here, we ran the same global analysis for each peptide and determined that the peptides offered similar diffusion lengths at 10:1 Peptide:(PPIX)Zn, between 5 and 10 nm, Figure S7, Table S2.

The short L_D values are not surprising because diffusion length directly correlates to the gross morphology (e.g. 1D nanofiber) which, as discussed, does not vary greatly along the length scale of exciton diffusion (< 10 nm). All of the assemblies yield similar hydrocarbon rich environments surrounding the pathway of diffusion suggesting that the microviscosity and local dielectric (which do not vary substantially in the series studied here) have a greater impact on exciton diffusion than chromophore ordering. Furthermore, L_D was noted to be shortened by excimer formation which has been observed to form in all peptides studied here.

The variations of microenvironment created by the X_3 variants were noticed to impact specifically the lifetime of excimer formation (τ_a) and decay ($\tau_{excimer}$), Table 1. To form the excimer, two (PPIX)Zn molecules must orient themselves in a precise geometry. Poorly ordered chromophore arrays will yield greater degrees of chromophore motility. As a result, the excimer will form faster. Our UV/vis and CD data suggest that L_3 yields the greatest degree of exciton coupling suggesting a high degree of ordering in the ground state which increases the time it takes to transition to the excimer (τ_a, table 1). Upon excitation, two neighboring (PPIX)Zn molecules in the L_3 array must move out of their highly ordered ground state into the excimer state which yields a slower excimer association rate when compared to the disordered arrays.

As mentioned earlier, the X_3 series yields a material that functions "in between" that of (PPIX)Zn functionalized myoglobin and a synthetic PZn array, Figure 6. By itself, (PPIX)Zn in buffer yields aggregates that emit at 660 nm, Figure 6A. Time resolved photoluminescence reveals a biexponential decay (τ_1 = 590 fs, τ_2 = 4.7 ps) with no observable rise time. In PZn molecular assemblies/aggregates, short picosecond lifetimes are indicative of exciton hopping between porphyrin units in a cofacial dimer.[36, 45] Picosecond hopping lifetimes ($\tau_{hopping}$ = 4.6 – 21 ps) depend greatly on the number of dimers in a given assembly as well as the distance between the dimers that is dictated by the covalent bridge between the cofacial dimer units. These hopping rates are not observed when (PPIX)Zn is bound to myoglobin as indicated by the observed intersystem crossing (τ_{ISC} = 2.2 ns) forming a long lived triplet state, Figure 6B.[44] The peptides studied here can induce a variety of porphyrin interactions as a function of sequence, causing a number of stacking and excimer formation interactions (Figure 6C). As a result, we observe excimer association rate constants (τ_a) that are larger than the exciton hopping values determined for the PZn molecular aggregates. As opposed to the rigid nature of the PZn molecular assemblies, our peptide nanofibers control the orientation of neighboring chromophores but they require molecular rearrangement prior to the hopping event thus resulting in longer association lifetimes (τ_a) (Figure 6C). Ultimately, the subtle changes in amino acid content of c16-AH**X_3**K_3-CO_2H control the degree of cofactor arrangement thus altering the rates of excimer formation and decay.

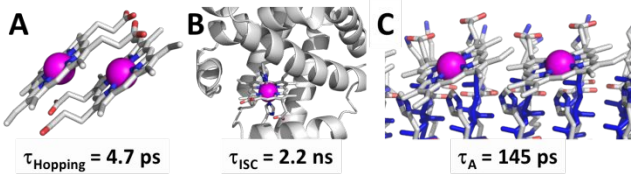

Figure 6. Illustrations depicting (A) a (PPIX)Zn dimer and short exciton hopping lifetime, (B) (PPIX)Zn:Mb highlighting the discrete metalloporphyrin binding pocket and the intersystem

crossing lifetime, and (C) the "in-between" state of the c16-AHL_3K_3-CO_2H:(PPIX)Zn assembly highlighting a long excimer association lifetime.

Conclusion

Light harvesting proteins exhibit precisely positioned chromophores for efficient transfer of energy towards catalytic processes essential in converting oxygen and carbon dioxide into useful fuels and foods. Here, we demonstrate precise control over the degree of molecular organization within a peptide construct thus highlighting the utility of self-assembled peptide materials for controlling light initiated processes. Specifically, we show that the photophysical properties of a very well-studied chromophore like (PPIX)Zn can be modulated via binding and incorporation into a series of self-assembled peptide materials, based on different amino acids proximal to the binding-site. In this work, we explored various physical properties when the microenvironment surrounding the cofactor binding site is varied. We demonstrate the following: (1) Binding affinity is heavily reliant on the size of the amino acid chain residues ($\mathbf{X_3}$ in c16-AH$\mathbf{X_3}K_3$-CO_2H) proximal to the (PPIX)Zn coordination site. To this affect, we identify that leucine and isoleucine yield the lowest dissociation constants (K_D), consistent with the designs for metalloporphyrin-binding peptide helical bundles. (2) Amino acid side chains dictate the degree of interchromophore interactions. L_3 exhibits the greatest splitting of the Soret band, the largest signal in CD spectroscopy, and the greatest excimer formation indicated by steady state photoluminescence spectroscopy. (3) Time resolved photoluminescence studies indicate that in spite of the varying degrees of interchromophore organization, each (PPIX)Zn:Peptide assembly affords observable excimer formation and similar kinetics with the key observation being represented by the singlet monomer association with the ground state to form the excimer (τ_a). With lifetime values varying between ~20 and 150 ps, the peptide assemblies demonstrate the

ability to mediate energy transfer processes between chromophores. The differences in lifetime occur because the aliphatic amino acids dictate the rate at which neighboring chromophores can orient themselves to facilitate excimer formation.

Demonstrating control over the photophysical processes of a chromophore like (PPIX)Zn by modulating its degree of organization within a peptide construct like c16-AH$\mathbf{X_3}K_3$-CO_2H is critical towards engineering novel photocatalytic materials. Exciton delocalization is a fundamental phenomenon for light harvesting in natural systems, but at some point that exciton needs to be used. This work is one step of the evolutionary path of this material toward functional chemistry from light energy. From here, peptide sequence changes can combine in ways that generate discrete points where interacting chromophores can produce chemical reactions. Therefore, our next challenge is to couple the observed light harvesting capabilities to an engineered catalytic site within the same peptide construct to further our efforts in developing functional light activated smart materials.

Materials and Methods

Peptide Design and Visualization: All peptides were designed with the assistance of hyperchem 8.0 modeling software. Upon construction, all amino acids were fixed to a parallel β-sheet conformation. The resulting monomeric peptides were then assembled into heptameric parallel β–sheet arrays with a ~ 6 Å intermolecular distances. One (PPIX)Zn molecule was axially coordinated to a single histidine via the δ-nitrogen. The assembly was then energy minimized (*in vac*uo) using CHARMM 27 force fields. Additional visualization was made possible using the freeware, PYMOL. The resulting structures were generated strictly for visualization/illustrative purposes.

Stock solution preparation: Each peptide (3-4 mg) was dissolved in nanopure water (Millipore A10) to obtain a 1 wt% solution (see the table below for final conentrations. Zinc protoporphyrin IX (Sigma-Aldrich) was dissolved in DMSO (Sigma Aldrich) to achieve a 10 mM stock solution. Note: (PPIX)Zn/DMSO stock solutions were always made to ensure that the final DMSO concentration in the sample was less than 1% (v/v). A 1 M ammonium hydroxide solution (diluted from concentrated ammonium hydroxide, Acros), was prepared for further dilution.

Molecular characterization – porphyrin binding: (PPIX)Zn was introduced to the 500 μM peptide solutions described in the previous section by adding 1.5 μL of the 10 mM (PPIX)Zn DMSO stock solution into the 300 μL peptide solution to yield 500 μM peptide, 50 μM (PPIX)Zn or 10:1 – peptide:(PPIX)Zn samples. The samples were then heated to 70 ^{o}C and cooled to room temperature.

For UV/visible spectroscopic analysis (Agilent Technologies, Cary 50 UV/visible spectrometer), the samples were transferred to a 1 mm quartz cuvette (Starna Cells, Inc.) and analyzed from 300 – 800 nm. Due to the size of some of the assemblies we observe some light scattering as evidenced by an increase in the baseline absorption. As a result, we correct for the sample

scattering by subtracting the absorption value at 800 nm. These same samples were analyzed by CD spectroscopy by scanning the Soret region from 350 – 500 nm. The secondary structure of the (PPIX)Zn coordinated assemblies were analyzed by IR spectroscopy only because the addition of DMSO UV cutoff precludes measurement in the 190 – 260 nm range required for CD measurements. Samples for IR were prepared in the same method described earlier when (PPIX)Zn is not coordinated to the assembly.

The titration experiments were performed as follows. In a 1 cm cuvette, 1.5 μL of the 10 mM (PPIX)Zn stock solution in DMSO was added to 3 mL of 30 mM NH_4OH. Aliquots of the 1 mM preassembled peptide solution were added in 5 μM aliquots to the 5 μM (PPIX)Zn solution. The peptide concentration was varied from 0 to 100 μM. The samples were monitored by UV/visible (Perkin Elmer Lambda 950) and fluorescence spectroscopy (Perkin Elmer).

Photophysical Characterization: All samples were prepared initially at a 10:1 peptide: (PPIX)Zn stoichiometry (500 μM:50 μM) in 30 mM NH_4OH. Time-resolved photoluminescence (trPL) data were acquired using a pulsed laser and streak camera detection system. Specifically, a 35-fs pulsewidth, amplified Ti:sapphire laser operating at 2 kHz pumped an optical parametric amplifier to produce 420 nm pump pulses which were directed into the sample. Any unbound (PPIX)Zn absorbs weakly in this region and therefore yields negligible signal relative to the signal from the bound state. Photoluminescence was collected with a lens and directed to a 150 mm focal length spectrograph and single-photon sensitive streak camera. The nitrogen-purged samples were stirred in a 2 mm quartz cuvette during the course of the measurement. The pump power was controlled by a variable neutral density filter and maintained within the linear excitation regime, well below the onset of exciton-exciton annihilation. Multiple measurements at varying pump power were performed for each sample for confirmation. For each power, measurements were performed with both a short (2 ns) and long

(10 ns) time window to capture both the fast dynamics of excimer formation and slow fluorescence decay of ZnP, and the datasets were subsequently merged.

Time-resolved measurements were performed with a commercial transient spectrometer (Newport Helios). Pump and probe pulses were derived from a regeneratively amplified Ti:sapphire laser (Newport Tsunami and SpitFire Pro), which produced 120-fs pulses at 5 kHz. Additional set-up information can be found in reference 38. The nitrogen purged samples were stirred in a 2 mm quartz cuvette during the course of the measurement. In the experiments reported within, we excited at 430 nm directly into the Soret band. The kinetic profiles were monitored at 515 nm. Each data set represents an average of three measurements. Data analysis was performed by fitting the kinetic to a biexponential decay profile (Origin 9).

Acknowledgments

This work was performed at the Center for Nanoscale Materials, a U.S. Department of Energy Office of Science User Facility, and supported by the U.S. Department of Energy, Office of Science, under Contract No. DE-AC02-06CH11357.

References

1. Y. Zeng, J. P. Chen, T. J. Yu, G. Q. Yang and Y. Li, *Acs Energy Letters*, 2017, **2**, 357-363.
2. J. Koepke, X. C. Hu, C. Muenke, K. Schulten and H. Michel, *Structure*, 1996, **4**, 581-597.
3. Y. Umena, K. Kawakami, J. R. Shen and N. Kamiya, *Nature*, 2011, **473**, 55-U65.
4. J. P. Dekker and E. J. Boekema, *Biochimica Et Biophysica Acta-Bioenergetics*, 2005, **1706**, 12-39.
5. R. Kouril, J. P. Dekker and E. J. Boekema, *Biochimica Et Biophysica Acta-Bioenergetics*, 2012, **1817**, 2-12.
6. D. Y. Yu, G. L. Zhu, S. Liu, B. S. Ge and F. Huang, *International Journal of Hydrogen Energy*, 2013, **38**, 16740-16748.
7. X. H. Liu, C. Liu, R. X. Sun, K. Liu, Y. J. Zhang, H. Q. Wang, J. F. Fang and C. H. Yang, *Acs Applied Materials & Interfaces*, 2015, **7**, 18904-18908.
8. C. J. Medforth, Z. C. Wang, K. E. Martin, Y. J. Song, J. L. Jacobsen and J. A. Shelnutt, *Chemical Communications*, 2009, DOI: 10.1039/b914432c, 7261-7277.
9. M. R. Wasielewski, *Accounts of Chemical Research*, 2009, **42**, 1910-1921.

10. J. Otsuki, *Journal of Materials A*, 2018, **6**, 6710-6753.
11. K. Oohora and T. Hayashi, *Current Opinion in Chemical Biology*, 2014, **19**, 154-161.
12. Q. L. Zou, K. Liu, M. Abbas and X. H. Yan, *Advanced Materials*, 2016, **28**, 1031-1043.
13. H. C. Fry, J. M. Garcia, M. J. Medina, U. M. Ricoy, D. J. Gosztola, M. P. Nikiforov, L. C. Palmer and S. I. Stupp, *Journal of the American Chemical Society*, 2012, **134**, 14646-14649.
14. L. A. Solomon, M. E. Sykes, Y. M. A. Wu, R. D. Schaller, G. P. Wiederrecht and H. C. Fry, *Acs Nano*, 2017, **11**, 9112-9118.
15. A. E. Counterman and D. E. Clemmer, *Journal of the American Chemical Society*, 1999, **121**, 4031-4039.
16. M. Lee, T. Wang, O. V. Makhlynets, Y. B. Wu, N. F. Polizzi, H. F. Wu, P. M. Gosavi, J. Stohr, I. V. Korendovych, W. F. DeGrado and M. Hong, *Proceedings of the National Academy of Sciences of the United States of America*, 2017, **114**, 6191-6196.
17. C. Negron, C. Fufezan and R. L. Koder, *Proteins-Structure Function and Bioinformatics*, 2009, **74**, 400-416.
18. J. Kong and S. Yu, *Acta Biochimica Et Biophysica Sinica*, 2007, **39**, 549-559.
19. S. M. Kelly, T. J. Jess and N. C. Price, *Biochimica Et Biophysica Acta-Proteins and Proteomics*, 2005, **1751**, 119-139.
20. C. J. Reedy and B. R. Gibney, *Chemical Reviews*, 2004, **104**, 617-649.
21. H. C. Fry, A. Lehmann, L. E. Sinks, I. Asselberghs, A. Tronin, V. Krishnan, J. K. Blasie, K. Clays, W. F. DeGrado, J. G. Saven and M. J. Therien, *Journal of the American Chemical Society*, 2013, **135**, 13914-13926.
22. N. F. Polizzi, M. J. Eibling, J. M. Perez-Aguilar, J. Rawson, C. J. Lanci, H. C. Fry, D. N. Beratan, J. G. Saven and M. J. Therien, *Journal of the American Chemical Society*, 2016, **138**, 2130-2133.
23. N. F. Polizzi, Y. B. Wu, T. Lemmin, A. M. Maxwell, S. Q. Zhang, J. Rawson, D. N. Beratan, M. J. Therien and W. F. DeGrado, *Nature Chemistry*, 2017, **9**, 1157-1164.
24. B. R. Gibney, F. Rabanal, K. S. Reddy and P. L. Dutton, *Biochemistry*, 1998, **37**, 4635-4643.
25. B. M. Discher, D. Noy, J. Strzalka, S. X. Ye, C. C. Moser, J. D. Lear, J. K. Blasie and P. L. Dutton, *Biochemistry*, 2005, **44**, 12329-12343.
26. F. V. Cochran, S. P. Wu, W. Wang, V. Nanda, J. G. Saven, M. J. Therien and W. F. DeGrado, *Journal of the American Chemical Society*, 2005, **127**, 1346-1347.
27. G. M. Bender, A. Lehmann, H. Zou, H. Cheng, H. C. Fry, D. Engel, M. J. Therien, J. K. Blasie, H. Roder, J. G. Saven and W. F. DeGrado, *Journal of the American Chemical Society*, 2007, **129**, 10732-10740.
28. K. A. McAllister, H. L. Zou, F. V. Cochran, G. M. Bender, A. Senes, H. C. Fry, V. Nanda, P. A. Keenan, J. D. Lear, J. G. Saven, M. J. Therien, J. K. Blasie and W. F. DeGrado, *Journal of the American Chemical Society*, 2008, **130**, 11921-11927.
29. H. C. Fry, A. Lehmann, J. G. Saven, W. F. DeGrado and M. J. Therien, *Journal of the American Chemical Society*, 2010, **132**, 3997-4005.
30. G. Kodali, J. A. Mancini, L. A. Solomon, T. V. Episova, N. Roach, C. J. Hobbs, P. Wagner, O. A. Mass, K. Aravindu, J. E. Barnsley, K. C. Gordon, D. L. Officer, P. L. Dutton and C. C. Moser, *Chemical Science*, 2017, **8**, 316-324.
31. J. L. Gao, H. Wang, Q. P. Yuan and Y. Feng, *Frontiers in Plant Science*, 2018, **9**, 7.
32. B. M. Fonseca, C. M. Paquete, C. A. Salgueiro and R. O. Louro, *Febs Letters*, 2012, **586**, 504-509.
33. L. C. Szymczak, H. Y. Kuo and M. Mrksich, *Analytical Chemistry*, 2018, **90**, 266-282.
34. I. Willner and E. Katz, *Angewandte Chemie-International Edition*, 2000, **39**, 1180-1218.
35. H. G. Cui, M. J. Webber and S. I. Stupp, *Biopolymers*, 2010, **94**, 1-18.
36. A. Satake and Y. Kobuke, *Organic & Biomolecular Chemistry*, 2007, **5**, 1679-1691.

37. S. Matile, N. Berova, K. Nakanishi, J. Fleischhauer and R. W. Woody, *Journal of the American Chemical Society*, 1996, **118**, 5198-5206.
38. N. Berova, L. Di Bari and G. Pescitelli, *Chemical Society Reviews*, 2007, **36**, 914-931.
39. K. Sauer, R. J. Cogdell, S. M. Prince, A. Freer, N. W. Isaacs and H. Scheer, *Photochemistry and Photobiology*, 1996, **64**, 564-576.
40. J. Adolphs, F. Muh, M. E. A. Madjet, M. S. A. Busch and T. Renger, *Journal of the American Chemical Society*, 2010, **132**, 3331-3343.
41. T. S. Balaban, *Accounts of Chemical Research*, 2005, **38**, 612-623.
42. L. L. Li and E. W. G. Diau, *Chemical Society Reviews*, 2013, **42**, 291-304.
43. S. Singh, A. Aggarwal, N. Bhupathiraju, G. Arianna, K. Tiwari and C. M. Drain, *Chemical Reviews*, 2015, **115**, 10261-10306.
44. L. Y. Luo, C. H. Chang, Y. C. Chen, T. K. Wu and E. W. G. Diau, *Journal of Physical Chemistry B*, 2007, **111**, 7656-7664.
45. N. Aratani, D. Kim and A. Osuka, *Accounts of Chemical Research*, 2009, **42**, 1922-1934.